

# Heterogeneity of Membrane Properties in Sympathetic Preganglionic Neurons of Neonatal Mice: Evidence of Four Subpopulations in the Intermediolateral Nucleus

Amanda Zimmerman<sup>1</sup> and Shawn Hochman<sup>2</sup>

<sup>1</sup>Department of Biomedical Engineering, Emory University/Georgia Institute of Technology; and <sup>2</sup>Department of Physiology, Emory University, Atlanta, Georgia

Submitted 17 July 2009; accepted in final form 9 November 2009

**Zimmerman A, Hochman S.** Heterogeneity of membrane properties in sympathetic preganglionic neurons of neonatal mice: evidence of four subpopulations in the intermediolateral nucleus. *J Neurophysiol* 103: 490–498, 2010. First published November 18, 2009; doi:10.1152/jn.00622.2009. Spinal cord sympathetic preganglionic neurons (SPNs) integrate activity from descending and sensory systems to determine the final central output of the sympathetic nervous system. The intermediolateral column (IML) has the highest number and density of SPNs and, within this region, SPN somas are found in distinct clusters within thoracic and upper lumbar spinal segments. Whereas SPNs exhibit a rostrocaudal gradient of end-target projections, individual clusters contain SPNs with diverse functional roles. Here we explored diversity in the electrophysiological properties observed in Hb9-eGFP-identified SPNs in the IML of neonatal mice. Overall, mouse SPN intrinsic membrane properties were comparable with those seen in other species. A wide range of values was obtained for all measured properties (up to a 10-fold difference), suggesting that IML neurons are highly differentiated. Using linear regression we found strong correlations between many cellular properties, including input resistance, rheobase, time constant, action potential shape, and degree of spike accommodation. The best predictor of cell function was rheobase, which correlated well with firing frequency–injected current ( $f$ - $I$ ) slopes as well as other passive and active membrane properties. The range in rheobase suggests that IML neurons have a recruitment order with stronger synaptic drives required for maximal recruitment. Using cluster analysis, we identified at least four subpopulations of SPNs, including one with a long time constant, low rheobase, and high  $f$ - $I$  gain. We thus propose that the IML contains populations of neurons that are differentiable by their membrane properties and hypothesize they represent diverse functional classes.

## INTRODUCTION

Sympathetic preganglionic neurons (SPNs) integrate activity from descending and sensory systems to determine the final central output of the sympathetic nervous system. The ILp (also known as the intermediolateral column or nucleus [IML]) has the highest number and density of SPNs (Petras and Cummings 1972; Rando et al. 1981) and, within this region, SPN somas are found in distinct clusters in each spinal segment. Their dendrites are mainly oriented rostrocaudally within the lateral funiculus and to a lesser extent medially within the gray matter toward the central autonomic area in lamina X, thus forming a ladder-like distribution symmetric around the central canal (Anderson et al. 1989; Sah and McLachlan 1995). SPNs are segmentally organized and exhibit a rostrocaudal gradient of end-target projections, yet individual clusters contain SPNs with diverse functional roles (Forehand et al. 1994).

Address for reprint requests and other correspondence: S. Hochman, Whitehead Biomedical Research Building, Room 644, Emory University School of Medicine, 615 Michael St., Atlanta, GA 30322 (E-mail: shawn.hochman@emory.edu).

The cellular physiological properties of SPNs that lie in the IML have been investigated in rats, guinea pigs, and cats to some extent (Dembowsky et al. 1985; Gilbey and Stein 1991; Inokuchi et al. 1993; Pickering et al. 1991; Sah and McLachlan 1995; Spanswick and Logan 1990b), largely using thick transverse (400 to 500  $\mu$ m) slices in vitro. Action potentials (APs) are notable for long afterhyperpolarizations (AHPs) mediated largely by  $\text{Ca}^{2+}$ -dependent transient- and sustained  $\text{K}^{+}$  conductances. Other conductances observed include: a fast 4-aminopyridine-sensitive and slower  $\text{Ba}^{2+}$ -sensitive transient outward rectifier (A-type and D-type, respectively), an atypical  $\text{K}^{+}$ -mediated sustained outward rectifier with insensitivity to  $\text{Cs}^{+}$  and tetraethylammonium, an anomalous inward rectifier, and a low-voltage activated T-type  $\text{Ca}^{2+}$  conductance (Miyazaki et al. 1996; Sah and McLachlan 1995; Wilson et al. 2002). Although IML SPNs are traditionally treated as a homogeneous group, there are some notable electrophysiological differences. Spontaneous activity has been observed in a subset of SPNs in the neonatal rat and adult guinea pig and is sometimes rhythmic (Spanswick and Logan 1990a). Additionally, strong electrical interactions have been observed in a subpopulation of SPNs, resulting in a low input resistance in these neurons (Logan et al. 1996). Finally, a number of investigators report mixed actions of the monoamines on SPNs (Gilbey and Stein 1991; Gladwell and Coote 1999; Yoshimura and Nishi 1982; Yoshimura et al. 1987c,d), suggesting different populations may have different receptor configurations.

Recently, an enhanced green fluorescent protein (eGFP)-labeled transgenic mouse (JAX Mice and Services, The Jackson Laboratory, Bar Harbor, ME) has been generated that identifies SPNs based on coupled expression to the HB9 homeodomain protein (Wilson et al. 2005), greatly facilitating ease of identification for electrophysiological and histochemical analyses. The current study represents the first characterization of membrane properties of SPNs in this mouse model and provides the first detailed appraisal of SPN repetitive firing properties. Last, we propose a novel classification scheme to differentiate SPN populations based on their electrophysiological properties.

A portion of these data was previously reported in abstract form (Zimmerman and Hochman 2008).

## METHODS

All procedures described here comply with the principles of The Care and Use of Animals outlined by the American Physiological Society and were approved by the Emory University Institutional Animal Care and Use Committee.

### Electrophysiology and slice preparation

All experiments were performed in transgenic mice expressing HB9-eGFP (known to label SPNs; JAX Mice and Services), postnatal day 3 (P3) to P9. Animals >P6 were anesthetized with 10% urethane (2 mg/kg, administered intraperitoneally) and placed on ice to slow the heart rate. All animals were decapitated and eviscerated and the spinal cords were removed. The T8–L2 section of the spinal cord was isolated and sliced into thick transverse (400  $\mu\text{m}$ ) and thin horizontal (200  $\mu\text{m}$ ) sections using a vibrating blade microtome (Leica VT1000S). Initial removal of the spinal cord and slicing were performed in cooled (4°C), oxygenated (95% O<sub>2</sub>-5% CO<sub>2</sub>) solution containing (in mM) 250 sucrose, 2.5 KCl, 2 CaCl<sub>2</sub>, 1 MgCl<sub>2</sub>, 25 glucose, 1.25 NaH<sub>2</sub>PO<sub>4</sub>, and 26 NaHCO<sub>3</sub> (pH 7.4). Slices were allowed to recover for  $\geq 1$  h.

The recording chamber was continuously perfused with oxygenated artificial cerebrospinal fluid containing (in mM): 125 NaCl, 2.5 KCl, 2 CaCl<sub>2</sub>, 1 MgCl<sub>2</sub>, 25 D-glucose, 1.25 NaH<sub>2</sub>PO<sub>4</sub>, and 26 NaHCO<sub>3</sub> (pH 7.4), at a rate of about 2 ml/min. Patch-clamp recordings were made from fluorescently identified SPNs with patch pipettes of resistance 4–8 M $\Omega$ . The standard intracellular recording solution contained (in mM): 140 K-gluconate, 0.2 EGTA, 10 HEPES, 4 Mg-ATP, and 1 Tris-GTP (pH 7.3). GTP and ATP were included in pipettes to prevent rundown of evoked currents. When assessing the effects of intracellular Cs<sup>+</sup>, the intracellular solutions contained (in mM) 140 CsF, 11 EGTA, 35 KOH, 10 HEPES, and 1 CaCl<sub>2</sub> (pH 7.3).

Whole cell patch-clamp recordings were undertaken at room temperature using the Multiclamp amplifier (Molecular Devices, Sunnyvale, CA). eGFP<sup>+</sup> SPNs were identified using epifluorescent illumination and their location in the intermediolateral column using differential-interference contrast (DIC) optics. Voltage- and current-clamp data were acquired on the computer using pClamp 10 acquisition software (Molecular Devices).

### Quantification of membrane properties

Immediately after rupture of the cell membrane (in voltage clamp at  $-90$  mV), the current-clamp recording configuration was used to determine resting membrane potential. Junction potential was corrected for after recording, experimentally derived previously to be 10 mV (MacLean et al. 1997). In current-clamp configuration, electrode resistance was compensated for, ranging from 8 to 15 M $\Omega$ . Unless otherwise noted, cells were brought to a  $-70$  mV holding potential by injecting bias current and a series of hyperpolarizing and depolarizing current steps 1 s in duration were applied. The membrane time constant ( $\tau_m$ ) was found by fitting the first 500 ms of the membrane charging response to small hyperpolarizing current steps with one or two exponentials. In cases where the data were better fit with two exponentials, the longest exponential was used as  $\tau_m$ , as suggested by Rall (1969) and previously calculated in SPNs (Pickering et al. 1991; Wilson et al. 2002). Additionally in these cases, the equivalent cylinder electrotonic length  $L$  was estimated using the formula:  $L = \pi(\tau_0/\tau_1 - 1)^{-1/2}$ , where  $\tau_0$  is  $\tau_m$  and  $\tau_1$  refers to the first equalizing time constant (Rall 1969).  $\tau_m$  was averaged for hyperpolarizing current steps causing a change in membrane potential  $<20$  mV. Current–voltage ( $I$ – $V$ ) plots were generated from voltage-clamp recordings. Electrode series resistance was uncompensated in voltage-clamp recordings, but was subtracted in current-clamp recordings. Series resistance values ranged between 15 and 38 M $\Omega$ . Because these values are one to two orders of magnitude less than measured membrane resistance, the uncompensated voltage drop across the electrode should not introduce significant error. In voltage-clamp mode, cells were held at  $-90$  mV and a series of voltage steps ( $-140$  to  $0$  mV, 500 ms duration) were applied. The input resistance ( $R_{in}$ ) was calculated by fitting a portion of the steady-state  $I$ – $V$  curve slightly negative to resting membrane potential ( $-70$  to  $-90$  mV) with a straight line. Membrane capacitance ( $C_m$ ) was determined automatically from Multiclamp Commander, by fitting the capacitive transient to a brief 10 mV voltage step and using the formula:

$\tau_m = R_{in} \times C_m$ . Peak inward current was measured as the maximal transient inward current obtained following voltage steps.

Active properties were averaged for all spikes at the lowest spike-triggering current step. The threshold voltage ( $V_{th}$ ) was determined by detecting the maximum second derivative in phase space ( $dV_m/dt$  vs.  $V_m$ ) for each spike (Sekerli et al. 2004). The spike amplitude and AHP magnitude were taken from this voltage threshold and the spike overshoot was calculated as the portion of the spike  $>0$  mV. Duration of the AP was measured as the time above one third of the amplitude (Wilson et al. 2002). Duration of the AHP was measured as the time below one tenth of the AHP magnitude. Rheobase was the minimum current injection required to elicit a spike. For frequency–current ( $f$ – $I$ ) analyses, both mean frequency and instantaneous frequency (based on the interspike interval between the first two spikes) were found. Data from neurons not showing electrode compensation in current clamp were discarded.

### Statistical analysis

All parameter values are reported as means  $\pm$  SD. Matlab software was used to compute correlation coefficients between membrane properties and to determine  $P$  values for each correlation. Unless otherwise noted, only those with  $P < 0.05$  were used. For some parameters with statistically significant correlations, linear regression with a least-squares fit was computed for either a straight line,  $y = mx + b$ , or logarithmic line,  $y = bm^x$ .

Cluster analysis was performed using a partition around medoids (PAMs) method (Kaufman and Rousseeuw 1990) from LIBRA (a MATLAB Library for Robust Analysis). In short, the PAM method minimizes the sum of dissimilarities between data points, to partition data into  $k$  clusters. This algorithm was run on  $k = 2$ – $10$  clusters, with each parameter normalized and centered. Both the Calinski–Harabasz (Calinski and Harabasz 1974) and Silhouette (Kaufman and Rousseeuw 1990) indices were calculated for each cluster number, each giving a weighted comparison between intra- and intercluster differences. These indices were maximized to determine the optimal number of data clusters.

## RESULTS

### General membrane properties

No significant difference in membrane properties was seen between thin horizontal and thick transverse slices, so the data were combined. Data were obtained from 39 neurons and membrane properties quantified as described in METHODS. Their properties are summarized in Table 1. The mean resting potential ( $V_{rest}$ ) was  $-60 \pm 7$  mV, ranging between  $-44$  and  $-85$  mV. The input resistance ( $R_{in}$ ) was  $1.1 \pm 0.6$  G $\Omega$ , ranging

TABLE 1. Summary of membrane properties

Property	Mean $\pm$ SD	$n$
Resting membrane potential, mV	$-59.8 \pm 7.4$	38
Input resistance, G $\Omega$	$1.14 \pm 0.6$	38
Time constant, ms	$92.4 \pm 43.7$	30
Capacitance, pF	$32.8 \pm 14.1$	25
Action potential		
Amplitude, mV	$57.1 \pm 8.9$	30
Overshoot, mV	$11.8 \pm 9.6$	30
Duration, ms	$6.3 \pm 1.4$	30
Threshold voltage, mV	$-45.3 \pm 5.8$	30
Rheobase, pA	$32.7 \pm 21.4$	30
Afterhyperpolarization		
Magnitude, mV	$15.2 \pm 3.6$	30
Duration, ms	$253.3 \pm 124.5$	23

from 260 M $\Omega$  to 2.6 G $\Omega$ , with an approximately normal distribution but with a greater spread in high resistance values (not shown). The mean membrane time constant ( $\tau_m$ ) was  $92 \pm 44$  ms, ranging between 36 and 184 ms, with an apparent bimodal distribution (not shown). Frequently, voltage responses to large current pulses were well fit with single exponentials, yet smaller current steps were better fit with double exponentials, also seen in the neonatal rat (Pickering et al. 1991). For those charging curves where double-exponential fits were easily distinguished, electrotonic length  $L$  was estimated to be  $1.83 \pm 0.27$  ( $n = 17$ ).  $R_{in}$  correlated well with both  $\tau_m$  ( $\rho = 0.65$ ,  $P = 0.001$ ) and  $C_m$  ( $\rho = -0.50$ ,  $P = 0.01$ ), indicating that variations in both membrane resistivity and cell size account for much of the range of resistances seen.

The relationships among and between active and passive membrane properties were quantified (Fig. 1). A color-coded correlation matrix compared significance of correlations among the membrane properties measured. The best predictor of cell function was rheobase, which accounted for 10.5% of the variance seen. Rheobase was positively correlated with threshold voltage ( $V_{th}$ ); negatively correlated with  $R_{in}$ ,  $\tau_m$ , and peak inward current ( $I_{peak}$ ); and weakly negatively correlated with both mean and instantaneous firing frequency–injected current ( $f$ - $I$ ) slopes, which fell just shy of statistical significance ( $\rho = -0.33$ ,  $P = 0.08$  for both). The early peak inward current (presumably Na<sup>+</sup> dominated) contributed appreciably to the cell's active properties because  $I_{peak}$  was inversely correlated to both  $V_{th}$  and rheobase. Additionally, AP height was inversely correlated to AP width and directly correlated to  $V_{th}$ ,

further highlighting the important role of Na<sup>+</sup> channel kinetics in SPN behavior. Last, the pronounced AHP magnitude was directly correlated to both mean and instantaneous  $f$ - $I$  slopes, suggesting a strong modulatory role of the underlying currents on SPN excitability.

Although not shown in the figure, age of the mouse used was also a factor, showing a strong positive correlation with  $I_{peak}$  ( $\rho = 0.73$ ,  $P = 3e^{-5}$ ), a weaker positive correlation with AHP magnitude ( $\rho = 0.43$ ,  $P = 0.05$ ), and a negative correlation with  $\tau_m$  ( $\rho = -0.40$ ,  $P = 0.03$ ). This would suggest that as the mouse ages, the density of voltage-gated Na<sup>+</sup> and K<sup>+</sup> channels increases and membrane resistivity decreases, a pattern supported by motoneuron research (O'Dowd et al. 1988; Viana et al. 1994).

#### Anomalous inward rectification

We next examined evidence of voltage-gated channels observed in these neurons compared with those reported previously in guinea pig and rat. In current-clamp mode, a number of SPNs exhibited an inward rectification or a fall in input resistance in response to larger hyperpolarizing current steps. This rectification was further explored and quantified in voltage clamp. In response to 500 ms voltage steps ( $-130$  to  $0$  mV, 10-mV steps), 24/38 SPNs (63%) exhibited an increased conductance (mean change: 492 pS) at membrane potentials less than  $-80$  mV (Fig. 2B). This conductance was instantaneous and sustained and was consistent with that seen in the neonatal rat (Wilson et al. 2002).

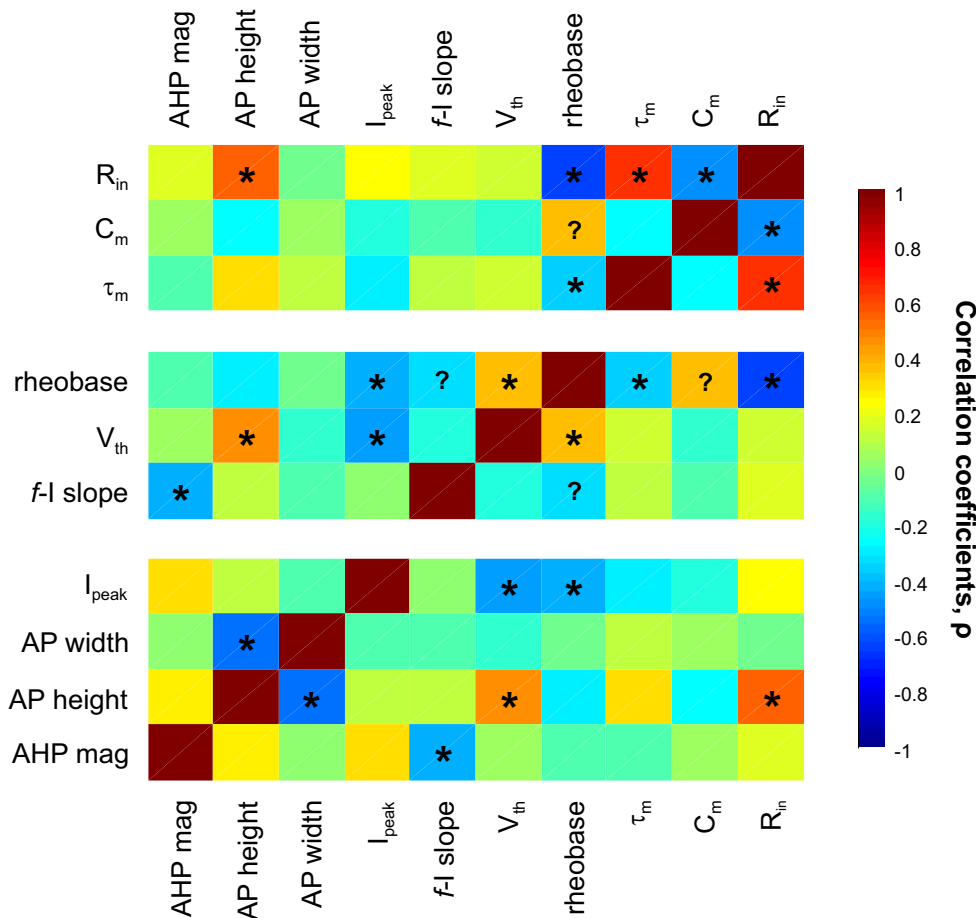


FIG. 1. Membrane property correlations. Figure shows correlation coefficients between membrane properties, with  $\rho$  values close to 1 showing strong positive relationships and  $\rho$  values close to  $-1$  showing strong negative relationships. The firing frequency–injected current ( $f$ - $I$ ) slope refers to instantaneous firing frequency. Asterisks (\*) denote statistically significant correlations ( $P < 0.05$ ) and “?” denotes correlations with  $0.05 < P < 0.1$ .

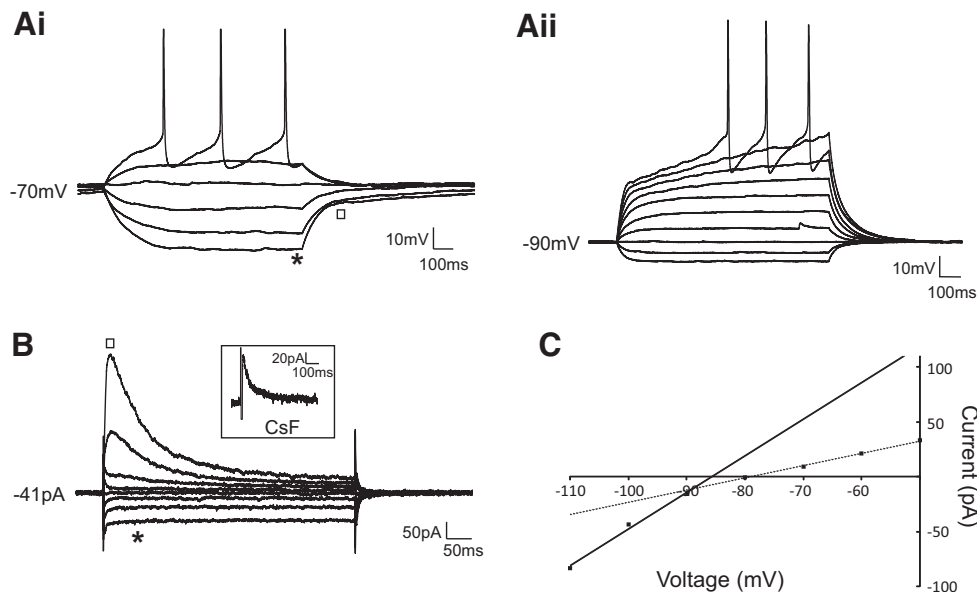


FIG. 2. Transient outward and anomalous rectification. *Ai*: sample membrane response to a series of current steps (1-s duration, -15 to 10 pA, 5-pA steps), holding current -12.6 pA. Asterisk (\*) indicates anomalous inward rectification; □ indicates transient outward rectification, seen as a much longer repolarization time to hyperpolarizing current steps. *Aii*: sample voltage response to a series of injected current pulses (1-s duration, 10-pA steps) from a hyperpolarized holding potential. Note delay to first spike, due to transient outward conductance. *B*: sample current response to a series of voltage-clamp steps (-30 to +40 mV, 10-mV steps) from a hyperpolarized holding potential of -90 mV. Asterisk (\*) indicates instantaneous increased conductance at hyperpolarized membrane potentials; □ indicates transient outward conductance, here activated at -70 mV and more pronounced at -60 and -50 mV. Next voltage step (-40 mV) produced an inward action current (not shown). *Inset* shows sample current response of a different cell to a -50-mV voltage step, when Cs<sup>+</sup> replaced intracellular K<sup>+</sup>. Note the presence of the transient outward conductance. *C*: sample current-voltage plot of steady-state currents obtained during voltage-clamp recordings, revealing inward rectification at potentials less than about -80 mV.

### Transient outward rectification

As seen in the guinea pig and rat (Inokuchi et al. 1993; Miyazaki et al. 1996; Wilson et al. 2002), all neurons displayed a transient outward rectification. This could be seen in current clamp either as a delayed return to resting membrane potential from hyperpolarizing current steps (10–40 pA, 1 s duration; Fig. 2*Ai*) or as a delay in time to fire the first AP with depolarizing current steps from a hyperpolarized membrane potential of -90 mV (Fig. 2*Aii*). This was further investigated in voltage-clamp configuration, where voltage steps (500 ms, 10 mV steps) were applied from a hyperpolarized holding potential (-90 mV). An outward transient current was observed with mean onset of  $-50.0 \pm 6.7$  mV and always with a lower threshold than that of the sodium spike (Fig. 2*B*). Decay was best fit by double exponentials, with the longest tau at onset of  $160 \pm 52$  ms. At least a portion of this transient outward current noticeably persisted when Cs<sup>+</sup> replaced K<sup>+</sup> in the intracellular solution ( $n = 6$ ; Fig. 2*B*, *inset*).

### Repetitive firing

In current-clamp mode from a -70 mV holding potential, 90% (39 of 43) of SPNs fired repetitively over a wide range of current injections, with the remaining 4 displaying an initial burst or single spike phenotype. Frequency-current ( $f$ - $I$ ) relationships were measured for both instantaneous and mean firing frequency at each current step. SPN  $f$ - $I$  instantaneous slopes had a mean value of  $0.228 \pm 0.125$  Hz/pA, with lower values for mean  $f$ - $I$  slope ( $0.196 \pm 0.106$  Hz/pA). Peak firing frequencies in individual neurons reached  $\leq 28$  Hz before depolarization block occurred.

Of SPNs firing repetitively, 70% (21 of 30) displayed spike-frequency adaptation (SFA) or a slowing of the firing rate with long current steps (Fig. 3*A*). SFA was best fit by a logarithmic linear regression (Fig. 3*B*) and only cells with established SFA are shown (fits significantly different from no correlation,  $P < 0.05$ ). The averaged slope ( $m$ ) of the logarithmic fit at each current step had a mean value of  $0.95 \pm 0.02$ . This slope was inversely correlated with input resistance—i.e., the greater the  $R_{in}$  value, the more rapidly spike frequency declined (Fig. 3*C*).

### Persistent inward current

When intracellular K<sup>+</sup> was replaced with Cs<sup>+</sup> to block most voltage-gated K<sup>+</sup> conductances, the steady-state  $I$ - $V$  plot revealed a region of negative slope conductance (Fig. 4*A*). This negative slope region indicates the presence of a persistent inward current (PIC) (Harvey et al. 2006). Net inward currents were absent in several neurons at least partly because of the presence of an outward leak conductance, but could be easily calculated as a deviation from linear leak slope (see Fig. 4*B*). The PIC in the presence of Cs<sup>+</sup> had an average onset of  $-76 \pm 5$  mV and peak magnitude  $21.6 \pm 13.5$  pA ( $n = 8$ ). Compared with K-gluconate intracellular solution, the effects of the PIC were largely hidden by the dominating contribution of activated outward currents during voltage steps, but could be detected during a slow voltage ramp (8 mV/s) as a slight deviation from the linear leak slope (Fig. 4*C*,  $n = 2/2$ ).

### Cluster analysis

Given the wide range of membrane properties recorded, we wondered whether SPNs could be classified into electrophys-

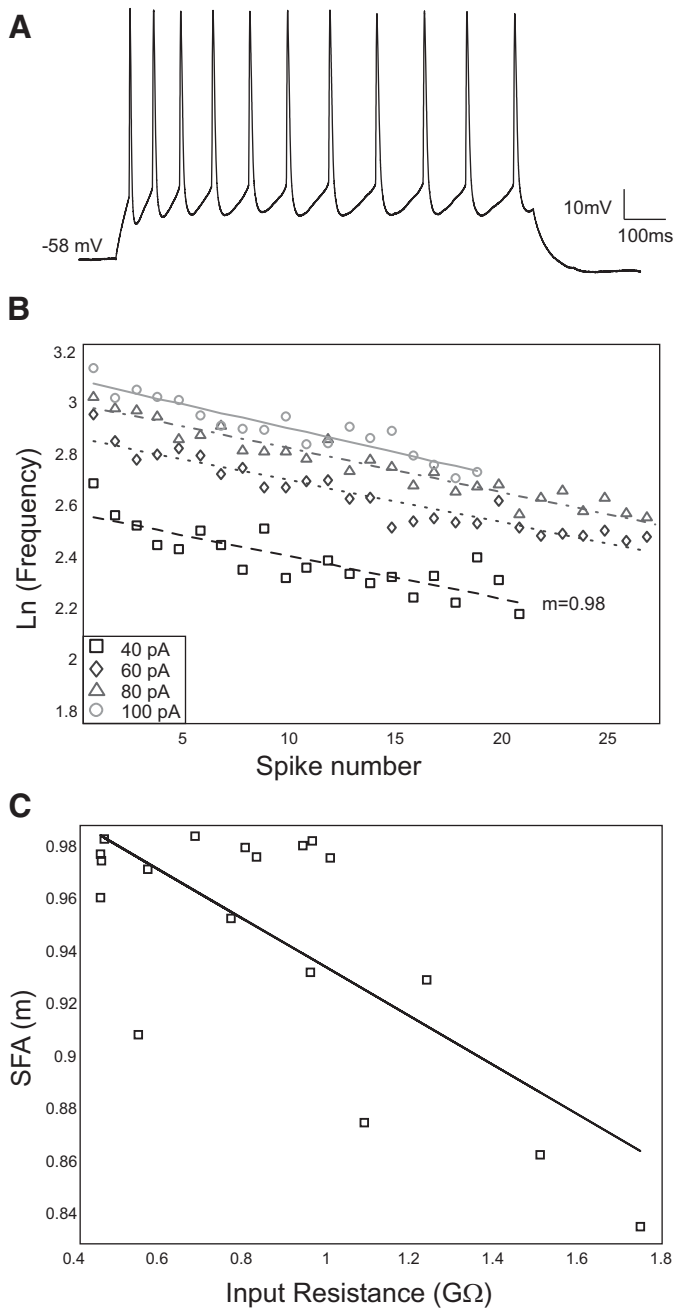


FIG. 3. Repetitive firing properties. *A*: sample response to 20-pA current injection (1-s duration). Note the slowing of the firing rate with each spike. *B*: frequency response of a typical sympathetic preganglionic neuron (SPN) showing spike-frequency adaptation (SFA) to multiple current injections, logarithmic scale.  $m$  was the natural log of the slopes of the lines shown. *C*: correlation between input resistance ( $R_{in}$ ) and SFA slope  $m$ , averaged for each cell. Only cells with statistically significant SFA are shown.

iological clusters. Using cluster analysis of the parameters measured for each cell and the maximum of the Silhouette and Calinski–Harabasz indices, data were best sorted into four clusters (Fig. 5*A*). A one-way ANOVA was performed on each parameter, resulting in statistically significant differences between clusters in  $\tau_m$ , rheobase,  $f$ - $I$  slopes, AP width, and  $I_{peak}$  (Fig. 5*B*). The mean values are summarized in Table 2. The four groups are as follows: group 2 and group 3 SPNs are recruited first (have lower rheobases), have relatively long  $\tau_m$

values, and midrange  $I_{peak}$  values. Group 2 neurons have lower  $f$ - $I$  gains and longer AP durations, whereas group 3 SPNs have higher  $f$ - $I$  gains and shorter AP durations. Group 1 and group 4 SPNs are then sequentially recruited, with group 1 SPNs having the largest and group 4 having the smallest  $I_{peak}$  values of all groups.

## DISCUSSION

Using eGFP-HB9-transgenics the present study undertook the first characterization of membrane electrical properties of sympathetic preganglionic neurons in the thoracolumbar intermediolateral nucleus of mouse. Studies were undertaken in

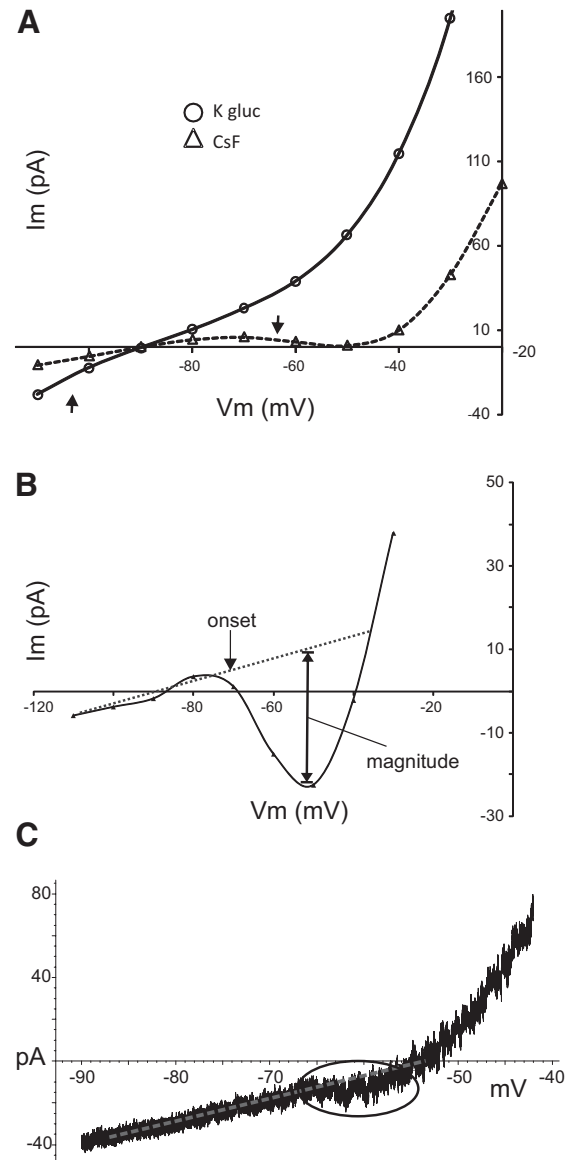


FIG. 4. Persistent inward currents (PICs). *A*: average steady-state current response to a series of 500-ms voltage steps with a CsF- and K-gluconate-based intracellular solution. Arrows denote the absence of anomalous rectifier and onset of negative slope conductance in CsF. *B*: sample neuron with a PIC resulting in negative conductance value, CsF-based intracellular solution. Arrows denote PIC onset and peak magnitude. *C*: PICs were largely masked by  $K^+$  conductances in K-gluconate-containing patch electrodes, but could be seen as small deviations from linear conductance during a slow voltage ramp (8 mV/s).

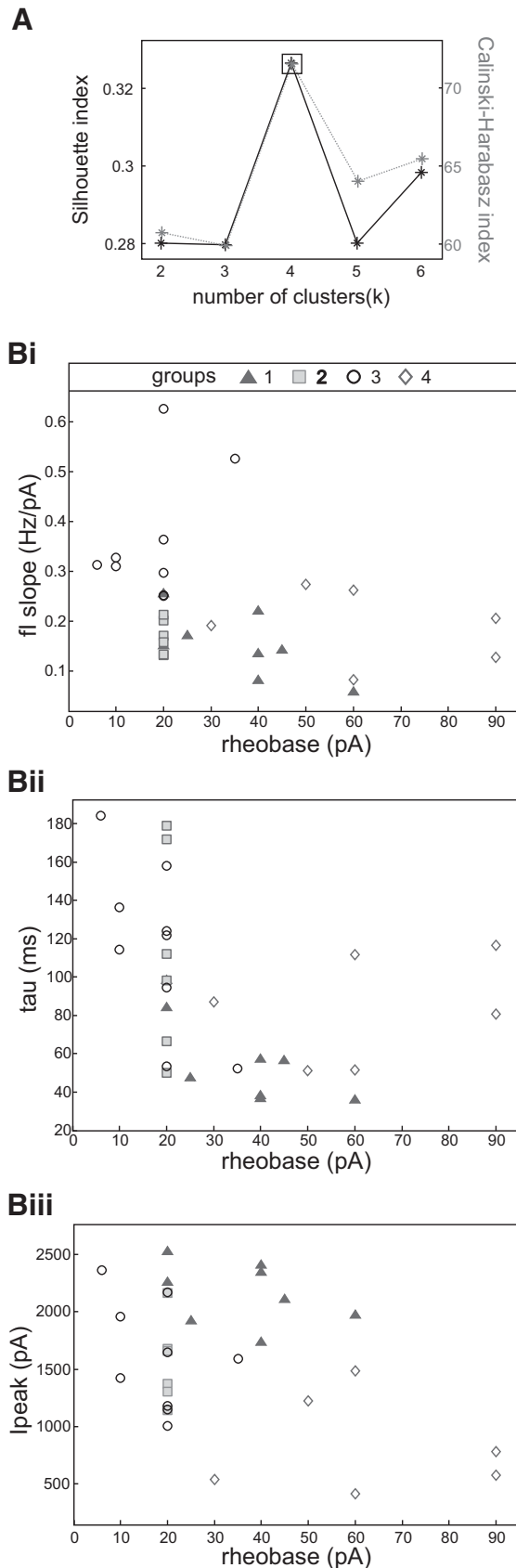


TABLE 2. Comparison of statistically significant parameter differences between clusters

Group	$\tau_m$ , ms	Rheobase, pA	$f-I$ Slope, Hz/pA
1	$56.7 \pm 23.1^3$	$36.3 \pm 13.8^{3,4}$	$0.15 \pm 0.07^3$
2	$112.9 \pm 53.1$	$20.0 \pm 0.0^4$	$0.17 \pm 0.03^3$
3	$115.5 \pm 43.8^1$	$17.9 \pm 8.5^1$	$0.36 \pm 0.13^{1,2,4}$
4	$83.1 \pm 28.2$	$63.3 \pm 23.4^{1,2}$	$0.19 \pm 0.08^3$

Group	$I_{peak}$ , pA	AP Width, ms	<i>n</i>
1	$2,157.8 \pm 270.3^{2,3,4}$	$5.3 \pm 0.7^2$	8
2	$1,553.9 \pm 363.4^{1,4}$	$8.1 \pm 1.6^{3,1}$	6
3	$1,608.0 \pm 473.7^{1,4}$	$5.9 \pm 1.0^2$	9
4	$837.3 \pm 426.8^{1,2,3}$	$6.7 \pm 0.6$	6

Superscripted numbers indicate statistically significant differences ( $P < 0.05$ ) from group noted.

either thicker transverse or thinner horizontal slices and membrane properties in these populations were indistinguishable. Given the strong rostrocaudal and mediolateral orientation of SPN IML dendrites, horizontal sections would be predicted to provide neurons with largely intact architecture. However, although mediolateral dendrites are strongly present in utero (Phelps et al. 1993), rostrocaudal projections have a relatively later maturation (2 wk postnatal; Ezerman and Forehand 1996; Markham et al. 1991), perhaps minimizing the level of dendrotomy in transverse slices at this age. Consequently, it is likely that the SPNs recorded in transverse sections retained considerable rostrocaudal dendrites.

A correlation matrix was used to identify relationships between active and passive membrane properties. One important observation was that rheobase—the amount of current required to recruit a neuron—was the best predictor of cell group and correlated with several other membrane properties. Given the obvious importance of SPN membrane excitability as the “final common CNS output” of sympathetic neural activity, we also undertook a detailed examination of their firing properties. SPNs consistently demonstrated spike-frequency adaptation. In addition, the relation of firing frequencies to magnitude of current injection ( $f-I$  relations) generated slopes that varied considerably across the SPN population, indicating that SPNs represent a highly differentiated class of neurons. Indeed, cluster analysis subdivided this nucleus into four subpopulations. The rostrocaudal range (T8–L2) sampled from potentially includes SPNs with five different end-target innervations (adrenal medulla, celiac ganglion, aorticorenal ganglion, superior mesenteric ganglion, and inferior mesenteric ganglion; Strack et al. 1988). Although outside the scope of the current study, it is possible this electrophysiological classification is influenced by end-target differentiation and warrants further investigation. Regardless, the overall conclusion is that this population of output neurons constitutes a heterogeneous

FIG. 5. Cluster analysis. A: analysis of cluster validity, using 2 different indices. Both indices peak at 4 clusters, signifying best fit for the data set. B: distribution of cluster membrane properties as a function of rheobase. Bi: groups 2 and 3 have low rheobase values, with group 3 having larger  $f-I$  gains. Groups 1 and 4 are sequentially recruited and can be largely distinguished by rheobase values. Bii: group 3 neurons have statistically larger  $\tau_m$  values than those of group 1 neurons. Biii: group 1 neurons display statistically larger  $I_{peak}$  values than those of both group 2 and group 3 SPNs and all have larger values than those of group 4 SPNs.

population, differentiated by their electrophysiological properties, with complex recruitment properties.

#### *Comparison with membrane properties reported in other species*

Membrane properties measured here compare well with those reported previously in other mammalian species. Resting membrane potential values were similar to those reported in the neonatal rat, guinea pig, and adult cat (Dembowsky et al. 1986; Inokuchi et al. 1993; Pickering et al. 1991; Yoshimura and Nishi 1982). Since impalement-induced leak conductance with sharp microelectrodes alters passive membrane properties (Staley et al. 1992), our whole cell patch recordings can be compared only with patch-clamp recordings as reported in the neonatal rat (Miyazaki et al. 1996; Pickering et al. 1991; Wilson et al. 2002). Similar input resistance ( $R_{in}$ ), membrane capacitance ( $C_m$ ), and membrane time constant ( $\tau_m$ ) values were observed [Miyazaki et al. 1996; Pickering et al. 1991; Wilson et al. 2002; but see Wilson et al. 2002 for temperature-dependent differences in  $R_{in}$ ]. The presence of multiple exponentials in the membrane charging curves in a number of neurons here was also reported in the neonatal rat (Pickering et al. 1991; Wilson et al. 2002). Multiple exponential responses are indicative of initial nonuniform distribution of membrane potential, likely due to a complex dendritic tree. Values obtained for  $L$  are much greater than those found in patch-clamp recordings from CA3 pyramidal neurons (Major et al. 1994) and even somatic motoneurons (Thurbon et al. 1998), known to have a very extensive dendritic arbor (Rekling et al. 2000). This suggests SPNs are not as electrically compact and their ability to integrate synaptic input from distal dendrites may be comparatively weak. The functional consequences of this are currently unknown.

The use of neonatal animals in the current study may be subject to criticism, given that the sympathetic nervous system of rodents is still maturing at this young age (Black 1978). Although end-target responses to central sympathetic activation are not present until after the first week postnatal, the level of tonic SPN activity and response to asphyxia and hypoglycemia in the neonate (1–2 days postnatal) were comparable with those in the adult rat (Smith et al. 1982). Additionally in the rat, as early as embryonic day 14.5 SPNs are already positioned in the IML, central autonomic region, and areas in between (Kubasak et al. 2004; Phelps et al. 1993). At birth, SPNs in the IML have the characteristic ladder-like rostrocaudal and mediolateral projecting dendritic arbor, with the rostrocaudal dendrites elongating and cluster separation increasing during the first 2 weeks (Ezerman and Forehand 1996; Markham et al. 1991; Phelps et al. 1984). Since biochemical markers of synaptic activity and synaptic connections in sympathetic ganglia in the mouse greatly increase during this period (Black et al. 1971), electrophysiological differentiation may play a role in forming appropriate synaptic connections. Interestingly, the similarity of the above-mentioned electrophysiological properties in the neonatal mouse to adult cats and more mature rats suggests that, whereas development may affect the size of SPNs and magnitude of conductances, the overall functional aspects of SPNs are largely in place in the neonate. Indeed, although this study used animals with an overlapping age range as undertaken in rat (as young as P7),

we also included even younger animals (P3) to demonstrate that SPN membrane properties are specified at a very early age. Moreover, cluster analysis was able to separate the IML neurons into at least four discrete groups irrespective of age. This is consistent with anatomical findings that morphology is also highly differentiated at birth (Phelps et al. 1984; Pyner and Coote 1994), supporting an early maturation of the IML SPN neuronal phenotype.

#### *Active conductances*

A transient outward rectification was present in virtually all SPNs as seen previously (Dembowsky et al. 1986; Inokuchi et al. 1993; Miyazaki et al. 1996; Pickering et al. 1991; Sah and McLachlan 1995; Wilson et al. 2002). This transient conductance was partially insensitive to intracellular  $Cs^+$ , inactive at resting membrane potential, and released from inactivation only with membrane hyperpolarization. In voltage-clamp mode, decay was best fit with double-exponential decay, consistent with the dual-component A-type  $K^+$  conductances noted by Wilson et al. (2002). In neonatal rat SPNs this current acts to regulate firing frequency and contributes to spike repolarization and afterhyperpolarization (Miyazaki et al. 1996). Hyperpolarizations from resting membrane potential evoked inward rectification in most SPNs and were sensitive to intracellular  $Cs^+$ . The conductance is similar to the anomalous rectification recorded in other SPNs (Inokuchi et al. 1993; Miyazaki et al. 1996; Pickering et al. 1991) and may act to return SPNs to an excitable membrane potential after large inhibitory input.

Blockade of most  $K^+$  conductances with  $Cs^+$  revealed the presence of a persistent inward current (PIC). In somatic motoneurons, PICs are thought to be responsible for repetitive firing and membrane bistability (Kuo et al. 2006; Lee and Heckman 1998). In our acute spinalized mouse SPNs, the PIC magnitude was usually small enough to be largely masked by outward  $K^+$  conductances with a  $K$ -gluconate-based intracellular solution. This may be due to the loss of descending monoaminergic input, which greatly facilitates PICs in motoneurons (Hounsgaard and Kiehn 1989; Lee and Heckman 1999). Given the strong descending monoaminergic projections to the IML, it is thus possible that SPNs also possess the ability for bistable membrane behavior.

#### *Repetitive firing and spike-frequency adaptation*

Neonatal mouse SPNs showed repetitive firing over a wide range of current injections. Compared with intracellular recordings in guinea pigs and cats, instantaneous firing rates and  $f-I$  slopes were much greater (Dembowsky et al. 1986; Inokuchi et al. 1993). This is likely at least partly due to a reduced leak conductance in patch-clamp recordings, compared with conventional sharp intracellular recordings (Staley et al. 1992). Compared with somatic motoneurons, SPN  $f-I$  gain exceeded that in both the primary and secondary firing range by 10-fold (Brownstone 2006), but this is also likely a reflection of substantially increased input resistance observed with patch-clamp recordings. Indeed, in patch-clamp recordings in putative mouse motoneurons in culture,  $f-I$  gains and variability were remarkably similar (Kuo et al. 2006). The strong correlation between the AHP magnitude and  $f-I$  gain found in the present study supports a functional role of the AHP (and

underlying conductances) in controlling cellular excitability. Modulation of the AHP, such as that in response to noradrenaline in both the cat and rat (Sah and McLachlan 1995; Yoshimura et al. 1987a) and caffeine in the rat (Shen et al. 1994), could lead to direct changes in SPN response to synaptic input.

In a majority of neonatal mouse SPNs, we describe a pronounced spike-frequency adaptation (SFA). SFA in SPNs has been reported previously (Dembowsky et al. 1986; Sah and McLachlan 1995), but has not been rigorously explored. In contrast, the mechanisms serving SFA have been detailed in mouse motoneurons (Miles et al. 2005). In this study, modeling and patch-clamp studies suggest that slow inactivation of the fast inactivating  $\text{Na}^+$  conductance is a key factor in SFA (Miles et al. 2005). This work contrasts previous notions on the primary importance of the AHP (see DISCUSSION in Miles et al. 2005). The physiological relevance of SFA in motoneurons has been interpreted in relation to initial versus sustained force generation in muscle (Stein and Parmiggiani 1979). Analogously, the relevance of SFA in SPNs may relate to the recruitment of postganglionic neurons. In our neonatal mouse SPNs, SFA decay was inversely related to  $R_{in}$ . Thus the smallest conductance neurons underwent the greatest SFA. Whether these neurons innervate a different population of postganglionic neurons or have differences in synaptic transmission remains to be determined.

The range of rheobase,  $R_{in}$ , and degree of SFA observed in SPNs could signify an organizational principle of recruitment with functional significance. For example, somatic motoneurons exhibit a well-defined order of recruitment via the size principle, whereby motoneurons are recruited with increasing size, conduction velocity, and motor unit fatigability (Henneman 1985; Reikling et al. 2000). In fact, lumbar SPNs in the adult cat have distinct differences in conduction velocity, responses to afferent stimuli, and voltage intensity for axonal recruitment based on their end-target innervations (Jänig and Szulczyk 1981).

SPNs normally fire at low frequencies (e.g., usually  $<1$  Hz, with peaks of 10 Hz; see McLachlan 2003) so it is worth questioning whether  $f-I$  curves are physiologically relevant at the higher range of firing frequencies. Peak firing frequencies observed here clearly exceed these steady-state values and many SPNs were not driven to their maximum firing potential. One possibility is that higher firing frequencies are reached during ischemia, drops in blood pressure, and states of higher arousal such as the “fight or flight” response. SPNs receive dense modulatory inputs from both brain stem and hypothalamic autonomic circuits (Anderson et al. 1989; Björklund and Skagerberg 1979; Fleetwood-Walker and Coote 1981; Loewy 1981), many of which could greatly increase their excitability on a systematic level. Indeed, addition of norepinephrine and serotonin has been shown to increase spontaneous discharge in SPNs in the neonatal rat (Lewis et al. 1993; Marks et al. 1990; Shen et al. 1994) and adult cat (Gilbey and Stein 1991; Yoshimura et al. 1987b), often in a bursting rhythm with intraburst frequencies greatly exceeding steady-state values.

Individual SPNs project to many postganglionic neurons (1:15 ratio in rat) and postganglionic neurons are innervated by multiple SPNs. The existence of both convergent and divergent synaptic inputs forming the postganglionic “autonomic motor unit” indicates the importance of synaptic integration in their

recruitment. Thus as a population, SPN firing properties will be critical in the temporal and spatial summation necessary to activate postganglionics. There appear to be two populations of SPNs based on synaptic strength on postganglionics—strong and weak—with strong synapses lacking P-type  $\text{Ca}^{2+}$  channels and evoking currents individually capable of recruiting postganglionics (McLachlan 2003). Thus recruitment of postganglionics may require the activity of only individual SPNs. Conversely, weak inputs from multiple SPNs may also be used to recruit postganglionic neurons. The relation between synapse strength and membrane properties remains to be determined. However, the initial high-frequency firing of SPNs could act to potentiate synaptic transmission of weak synaptic connections, whereas the slower firing induced by SFA could act to maintain potentiation without neurotransmitter depletion (McLachlan 1975).

In conclusion, the present study suggests that SPNs in the IML are comprised of multiple subtypes, easily distinguished by electrophysiological parameters. We hypothesize that generation of target- and condition-specific responses of the sympathetic nervous system is largely derived from electrophysiological differentiation. The easy visualization of SPNs afforded by their genetic labeling with Hb9-eGFP in transgenic mice allows for coupling future studies of electrophysiological results with immunohistochemistry, anatomy, and functional genomics for further exploration.

#### ACKNOWLEDGMENTS

We thank M. Sorenson for *readabf* and K. Wang for the *Cluster Validity Analysis Platform*, Matlab programs used in this analysis.

#### GRANTS

This work was supported by National Institute of Neurological Disorders and Stroke Grant NS-045248.

#### REFERENCES

- Anderson CR, McLachlan EM, Srb-Christie O. Distribution of sympathetic preganglionic neurons and monoaminergic nerve terminals in the spinal cord of the rat. *J Comp Neurol* 283: 269–284, 1989.
- Björklund A, Skagerberg G. Evidence for a major spinal cord projection from the diencephalic A11 dopamine cell group in the rat using transmitter-specific fluorescent retrograde tracing. *Brain Res* 177: 170–175, 1979.
- Black IB. Regulation of autonomic development. *Annu Rev Neurosci* 1: 183–214, 1978.
- Black IB, Hendry IA, Iversen LL. Trans-synaptic regulation of growth and development of adrenergic neurones in a mouse sympathetic ganglion. *Brain Res* 34: 229–240, 1971.
- Brownstone RM. Beginning at the end: repetitive firing properties in the final common pathway. *Prog Neurobiol* 78: 156–172, 2006.
- Calinski T, Harabasz J. A dendrite method for cluster analysis. *Commun Stat* 3: 1–27, 1974.
- Dembowsky K, Czachurski J, Seller H. An intracellular study of the synaptic input to sympathetic preganglionic neurones of the third thoracic segment of the cat. *J Auton Nerv Syst* 13: 201–244, 1985.
- Dembowsky K, Czachurski J, Seller H. Three types of sympathetic preganglionic neurones with different electrophysiological properties are identified by intracellular recordings in cat. *Pflügers Arch* 406: 112–120, 1986.
- Ezerman EB, Forehand CJ. Development and segmental organization of rostrocaudal dendrites of rat sympathetic preganglionic neurons. *J Auton Nerv Syst* 57: 29–35, 1996.
- Fleetwood-Walker SM, Coote JH. Contribution of noradrenaline-, dopamine- and adrenaline-containing axons to the innervation of different regions of the spinal cord of the cat. *Brain Res* 206: 95–106, 1981.
- Forehand CJ, Ezerman EB, Rubin E, Glover JC. Segmental patterning of rat and chicken sympathetic preganglionic neurons: correlation between soma position and axon projection pathway. *J Neurosci* 14: 231–241, 1994.

- Gilbey MP, Stein RD. Characteristics of sympathetic preganglionic neurones in the lumbar spinal cord of the cat. *J Physiol* 432: 427–443, 1991.
- Gladwell SJ, Coote JH. Inhibitory and indirect excitatory effects of dopamine on sympathetic preganglionic neurones in the neonatal rat spinal cord in vitro. *Brain Res* 818: 397–407, 1999.
- Harvey PJ, Li Y, Li X, Bennett DJ. Persistent sodium currents and repetitive firing in motoneurons of the sacrocaudal spinal cord of adult rats. *J Neurophysiol* 96: 1141–1157, 2006.
- Henneman E. The size-principle: a deterministic output emerges from a set of probabilistic connections. *J Exp Biol* 115: 105–112, 1985.
- Houngaard J, Kiehn O. Serotonin-induced bistability of turtle motoneurons caused by a nifedipine-sensitive calcium plateau potential. *J Physiol* 414: 265–282, 1998.
- Inokuchi H, Masuko S, Chiba T, Yoshimura M, Polosa C, Nishi S. Membrane properties and dendritic arborization of the intermediolateral nucleus neurons in the guinea-pig thoracic spinal cord in vitro. *J Auton Nerv Syst* 43: 97–106, 1993.
- Jänig W, Szulczyk P. The organization of lumbar preganglionic neurons. *J Auton Nerv Syst* 3: 177–191, 1981.
- Kaufman L, Rousseeuw PJ. *Finding Groups in Data: An Introduction to Cluster Analysis*. New York: Wiley-Interscience, 1990.
- Kubasak MD, Brooks R, Chen S, Villeda SA, Phelps PE. Developmental distribution of reelin-positive cells and their secreted product in the rodent spinal cord. *J Comp Neurol* 468: 165–178, 2004.
- Kuo JJ, Lee RH, Zhang L, Heckman CJ. Essential role of the persistent sodium current in spike initiation during slowly rising inputs in mouse spinal neurones. *J Physiol* 574: 819–834, 2006.
- Lee RH, Heckman CJ. Bistability in spinal motoneurons in vivo: systematic variations in persistent inward currents. *J Neurophysiol* 80: 583–593, 1998.
- Lee RH, Heckman CJ. Enhancement of bistability in spinal motoneurons in vivo by the noradrenergic alpha 1 agonist methoxamine. *J Neurophysiol* 81: 2164–2174, 1999.
- Lewis DI, Sermasi E, Coote JH. Excitatory and indirect inhibitory actions of 5-hydroxytryptamine on sympathetic preganglionic neurones in the neonate rat spinal cord in vitro. *Brain Res* 610: 267–275, 1993.
- Loewy AD. Raphe pallidus and raphe obscurus projections to the intermediolateral cell column in the rat. *Brain Res* 222: 129–133, 1981.
- Logan SD, Pickering AE, Gibson IC, Nolan MF, Spanswick D. Electrotonic coupling between rat sympathetic preganglionic neurones in vitro. *J Physiol* 495: 491–502, 1996.
- MacLean JN, Schmidt BJ, Hochman S. NMDA receptor activation triggers voltage oscillations, plateau potentials and bursting in neonatal rat lumbar motoneurons in vitro. *Eur J Neurosci* 9: 2702–2711, 1997.
- Major AD, Larkman AU, Jonas P, Sakmann B, Jack JJ. Detailed passive cable models of whole-cell recorded CA3 pyramidal neurons in rat hippocampal slices. *J Neurosci* 14: 4613–4638, 1994.
- Markham JA, Phelps PE, Vaughn JE. Development of rostrocaudal dendritic bundles in rat thoracic spinal cord: analysis of cholinergic sympathetic preganglionic neurons. *Dev Brain Res* 61: 229–236, 1991.
- Marks SA, Stein RD, Dashwood MR, Gilbey MP. [<sup>3</sup>H]Prazosin binding in the intermediolateral cell column and the effects of iontophoresed methoxamine on sympathetic preganglionic neuronal activity in the anaesthetized cat and rat. *Brain Res* 530: 321–324, 1990.
- McLachlan EM. An analysis of the release of acetylcholine from preganglionic nerve terminals. *J Physiol* 245: 447–466, 1975.
- McLachlan EM. Transmission of signals through sympathetic ganglia: modulation, integration or simply distribution? *Acta Physiol Scand* 177: 227–235, 2003.
- Miles GB, Dai Y, Brownstone RM. Mechanisms underlying the early phase of spike frequency adaptation in mouse spinal motoneurons. *J Physiol* 566: 519–532, 2005.
- Miyazaki T, Dun NJ, Kobayashi H, Tosaka T. Voltage-dependent potassium currents of sympathetic preganglionic neurons in neonatal rat spinal cord thin slices. *Brain Res* 743: 1–10, 1996.
- O'Dowd DK, Ribera AB, Spitzer NC. Development of voltage-dependent calcium, sodium, and potassium currents in *Xenopus* spinal neurons. *J Neurosci* 8: 792–805, 1988.
- Petras JM, Cummings JF. Autonomic neurons in the spinal cord of the rhesus monkey: a correlation of the findings of cytoarchitectonics and sympathectomy with fiber degeneration following dorsal rhizotomy. *J Comp Neurol* 146: 189–218, 1972.
- Phelps PE, Barber RP, Houser CR, Crawford GD, Salvaterra PM, Vaughn JE. Postnatal development of neurons containing choline acetyltransferase in rat spinal cord: an immunocytochemical study. *J Comp Neurol* 229: 347–361, 1984.
- Phelps PE, Barber RP, Vaughn JE. Embryonic development of rat sympathetic preganglionic neurons: possible migratory substrates. *J Comp Neurol* 330: 1–14, 1993.
- Pickering AE, Spanswick D, Logan SD. Whole-cell recordings from sympathetic preganglionic neurons in rat spinal cord slices. *Neurosci Lett* 130: 237–242, 1991.
- Pyner S, Coote JH. A comparison between the adult rat and neonate rat of the architecture of sympathetic preganglionic neurones projecting to the superior cervical ganglion, stellate ganglion and adrenal medulla. *J Auton Nerv Syst* 48: 153–166, 1994.
- Rall W. Time constants and electrotonic length of membrane cylinders and neurons. *Biophys J* 9: 1483–1508, 1969.
- Rando TA, Bowers CW, Zigmond RE. Localization of neurons in the rat spinal cord which project to the superior cervical ganglion. *J Comp Neurol* 196: 73–83, 1981.
- Rekling JC, Funk GD, Bayliss DA, Dong X-W, Feldman JL. Synaptic control of motoneuronal excitability. *Physiol Rev* 80: 767–852, 2000.
- Sah P, McLachlan EM. Membrane properties and synaptic potentials in rat sympathetic preganglionic neurons studied in horizontal spinal cord slices in vitro. *J Auton Nerv Syst* 53: 1–15, 1995.
- Sekerli M, Del Negro CA, Lee RH, Butera RJ. Estimating action potential thresholds from neuronal time-series: new metrics and evaluation of methodologies. *IEEE Trans Biomed Eng* 51: 1665–1672, 2004.
- Shen E, Wu SY, Dun NJ. Spontaneous and transmitter-induced rhythmic activity in neonatal rat sympathetic preganglionic neurons in vitro. *J Neurophysiol* 71: 1197–1205, 1994.
- Smith P, Slotkin TA, Mills E. Development of sympathetic ganglionic neurotransmission in the neonatal rat. Pre- and postganglionic nerve response to asphyxia and 2-deoxyglucose. *Neuroscience* 7: 501–507, 1982.
- Spanswick D, Logan SD. Spontaneous rhythmic activity in the intermediolateral cell nucleus of the neonate rat thoracolumbar spinal cord in vitro. *Neuroscience* 39: 395–403, 1990a.
- Spanswick D, Logan SD. Sympathetic preganglionic neurones in neonatal rat spinal cord in vitro: electrophysiological characteristics and the effects of selective excitatory amino acid receptor agonists. *Brain Res* 525: 181–188, 1990b.
- Staley KJ, Otis TS, Mody I. Membrane properties of dentate gyrus granule cells: comparison of sharp microelectrode and whole-cell recordings. *J Neurophysiol* 67: 1346–1358, 1992.
- Stein RB, Parmiggiani F. Optimal motor patterns for activating mammalian muscle. *Brain Res* 175: 372–376, 1979.
- Strack AM, Sawyer WB, Marubio LM, Loewy AD. Spinal origin of sympathetic preganglionic neurons in the rat. *Brain Res* 455: 187–191, 1988.
- Thurbon D, Luscher H-R, Hofstetter T, Redman SJ. Passive electrical properties of ventral horn neurons in rat spinal cord slices. *J Neurophysiol* 79: 2485–2502, 1998.
- Viana F, Bayliss DA, Berger AJ. Postnatal changes in rat hypoglossal motoneuron membrane properties. *Neuroscience* 59: 131–148, 1994.
- Wilson JM, Hartley R, Maxwell DJ, Todd AJ, Lieberam I, Kaltschmidt JA, Yoshida Y, Jessell TM, Brownstone RM. Conditional rhythmicity of ventral spinal interneurons defined by expression of the Hb9 homeodomain protein. *J Neurosci* 25: 5710–5719, 2005.
- Wilson JMM, Coderre E, Renaud LP, Spanswick D. Active and passive membrane properties of rat sympathetic preganglionic neurones innervating the adrenal medulla. *J Physiol* 545: 945–960, 2002.
- Yoshimura M, Nishi S. Intracellular recordings from lateral horn cells of the spinal cord in vitro. *J Auton Nerv Syst* 6: 5–11, 1982.
- Yoshimura M, Polosa C, Nishi S. Noradrenaline-induced afterdepolarization in cat sympathetic preganglionic neurons in vitro. *J Neurophysiol* 57: 1314–1324, 1987a.
- Yoshimura M, Polosa C, Nishi S. Noradrenaline induces rhythmic bursting in sympathetic preganglionic neurons. *Brain Res* 420: 147–151, 1987b.
- Yoshimura M, Polosa C, Nishi S. Slow EPSP and the depolarizing action of noradrenaline on sympathetic preganglionic neurons. *Brain Res* 414: 138–142, 1987c.
- Yoshimura M, Polosa C, Nishi S. Slow IPSP and the noradrenaline-induced inhibition of the cat sympathetic preganglionic neuron in vitro. *Brain Res* 419: 383–386, 1987d.
- Zimmerman A, Hochman S. Electrophysiological characterization of sympathetic preganglionic neurons in HB9-GFP transgenic mice. *Soc Neurosci Abstr* 34: 240.2/E24, 2008.